Atomistic Simulations of End-Linked Poly(dimethylsiloxane) Networks: Structure and Relaxation

David R. Heine,* Gary S. Grest, Christian D. Lorenz, Mesfin Tsige, and Mark J. Stevens

Sandia National Laboratories, Albuquerque, New Mexico 87185

Received November 24, 2003; Revised Manuscript Received March 11, 2004

ABSTRACT: The structure and elastic moduli of end-cross-linked poly(dimethylsiloxane) (PDMS) networks are studied using molecular dynamics (MD). The systems consist of 2000 PDMS chains of length 20 monomers and 1000 chains of length 40 monomers with varying amounts of cross-linker molecules. The networks are formed dynamically within the MD simulations. Starting from an equilibrated melt, tetrakis(dimethylsiloxy)silane cross-linkers are attached randomly to a fraction of the chain ends. When a free end comes within a short capture distance from an unsaturated cross-linker, a bond is formed between the chain and the cross-linker. The kinetics of the cross-linking process are studied as a function of the stoichiometry of the number of cross-linkers and are found to agree with earlier predictions. Stress relaxation simulations are performed on the fully formed networks by straining each system at four different rates and recording the tensile stress during the relaxation period. Results for the elastic moduli of the networks calculated from the plateau value of the tensile stress are compared to network models, and qualitative agreement with dynamic mechanical experiments is found. The chain conformations after straining indicate that these networks are deformed much more affinely than what is seen experimentally.

1. Introduction

The physics of cross-linked polymer networks has been extensively studied due to their industrial importance as rubbers and gels. Despite this effort, many questions concerning the behavior of polymer networks still remain. The earliest models of rubber elasticity, the affine model[1,2] and the phantom model,[3] apply to monodisperse networks and neglect both the excluded volume of the chain and entanglement effects. They differ in their treatment of the motion of cross-linkers. The affine model assumes that the cross-linkers are confined to fixed locations in the network and has been found to work in the small deformation limit. For the affine model, the shear modulus is given by

$$G^{\text{affine}} = \nu RT \tag{1}$$

where ν is the number of moles of chains per unit volume. The phantom model assumes that the cross-linkers can fluctuate freely about their mean positions in the network. In the phantom model, the shear modulus is given by

$$G^{\text{phantom}} = (\nu - \mu)RT \tag{2}$$

where μ is the number of moles of cross-linkers per unit volume. Uniaxial extension/compression and swelling experiments have shown that these models fail to predict the properties of real networks under realistic deformations.[4−6] In the constrained junction model,[7−9] fluctuations of the junctions in a phantom network are impeded by entanglements, giving a modulus that is intermediate between the affine and phantom models. The constrained junction model has been able to qualitatively predict the behavior of some real networks.[4,5,10] Other experiments[11,12] and simulations[13−17] have shown that interchain entanglements contribute significantly to the modulus, contrary to the constrained junction model. The tube model[18,19] considers the motion of each strand to be confined to a tube formed by the surrounding strands. This model, which originally showed the importance of reptation dynamics in entangled polymer melts, is equally valid as a description of polymer networks. It has recently been combined with the constrained junction model[20] to account for both effects in the network.

The chemical inertness and thermal stability of PDMS makes it well suited for many applications including adhesives, seals, coatings, and encapsulants. For the same reasons, it is frequently used in experimental investigations of polymer networks. To test the theories of rubber elasticity, experimentalists have investigated model networks, prepared by end-linking cross-linkers with a monodisperse sample of polymers. This approach allows the strand length and cross-link functionality to be controlled, but the extent of reaction has just as much influence on the properties of the network.[21,22] The maximum extent of reaction was found to be between 80% and 90% for PDMS cross-linked with phenyltris(dimethylsiloxy)silane.[23] This limits the ability to make direct comparisons with theoretical models since the bulk properties of the networks are strongly dependent on the number of free chain ends.

Molecular dynamics simulation is an attractive tool for studying polymer networks because of its ability to provide control over the details of the network in a much simpler way than through experimentation. MD simulations allow one to study the nature of stress on the atomic level and to quantify the effects of variables such as the strand length, extent of reaction, and chain topology on the physical properties of the network. This flexibility can be utilized to produce ideal networks useful for testing theoretical models or to produce realistic networks to provide additional insight into

* To whom correspondence should be addressed. E-mail drheine@sandia.gov.

10.1021/ma035760j CCC: $27.50
Published on Web 04/20/2004

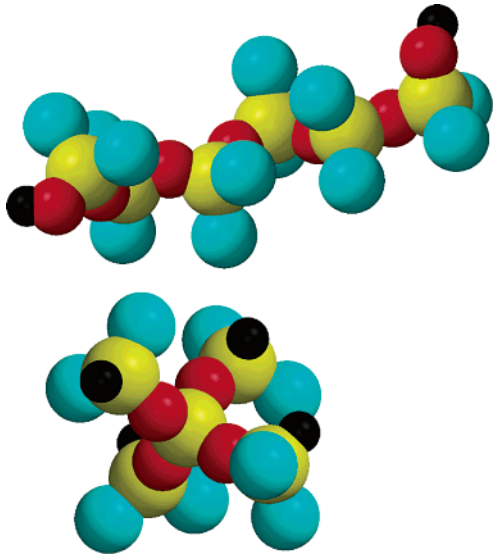

Figure 1. (top) Schematic representation of the united atom model for silanol-terminated poly(dimethylsiloxane): yellow (Si), red (O), cyan (CH_3), black (H). (bottom) Tetrakis(dimethylsiloxy)silane cross-linker molecule. The chain lengths used in the MD simulations are either 20 or 40 monomers per chain. Atom sizes in this figure are not to scale.

experimentally observed behavior. Although there have been a number of MD[13−15,24−27] and Monte Carlo simulations[16,28−31] of polymer networks, these studies have been on coarse-grained models, either in the continuum or on a lattice. Previously, there has been no simulation of polymer network formation and stress relaxation using atomistic models. An atomistic level of detail allows several practical problems to be explored in detail, including network formation near surfaces and in the presence of solvent.

This paper presents the first molecular dynamics simulations of polymer network formation at the united atom level. These simulations are intended as an evaluation of atomistic modeling of network formation. We present extensive MD results for the network formation and stress/strain behavior of PDMS end-cross-linked with tetrakis(dimethylsiloxy)silane cross-linkers. Details of the simulation are presented in section 2. The network formation procedure and resulting formation kinetics are discussed in section 3 in terms of diffusion-controlled kinetics. Uniaxial extension simulations and measurements of the moduli are in section 4. Results are also compared to data from dynamic mechanical experiments. Final discussions and conclusions are presented in section 5.

2. Simulation Details

The molecular structures of OH-terminated PDMS chains and tetrakis(dimethylsiloxy)silane cross-linkers are shown in Figure 1. In the presence of a catalyst, each cross-linker molecule is able to bond to four terminal hydroxy groups on the PDMS chains via the reaction

$$\mathrm{RH + HO{-}Si(CH_3)_2R' \rightarrow R{-}O{-}Si(CH_3)_2R' + H_2}$$

where R represents the cross-linker molecule and R′ represents the PDMS chain. Most model networks are prepared experimentally using vinyl-terminated PDMS chains, but as this is our first atomistic study of polymer networking and since the potentials are better characterized for silanol-terminated PDMS chains, we use silanol-terminated PDMS chains. This system is expected to give similar results for the structure and moduli as networks prepared by end-linking vinyl-terminated chains.

For the united atom model employed here, methyl groups (shown in blue) are treated as single interaction sites. Although Figure 1 shows hydrogen atoms on the terminal oxygen atoms, the hydrogen atoms are not explicitly included in the simulation. Hence, when the reaction occurs, no H_2 molecules are explicitly simulated. Similarly, no catalyst molecules are simulated. For the interaction parameters, we use a recently developed united atom force field[32] optimized to match the structure. With this force field, the mean-square radius of gyration and mean-square end-to-end distance are within 2.5% and 8.7%, respectively, of those for PDMS melts obtained from explicit atom simulations with class II potentials. The static structure factor, $S(q)$, is also found to be in good agreement with results from wide-angle X-ray scattering experiments.

The nonbond potential acts on each pair of sites on the same molecule separated by four or more bonds and all pairs of sites on different molecules. The interaction potential contains both van der Waals and Coulomb terms and is defined by[32]

$$U_{\alpha\beta}^{\mathrm{nonbond}}(r) = \begin{cases} U_{\alpha\beta}^{\mathrm{vdW}}(r) + k_q \dfrac{q_\alpha q_\beta}{r} & r < r_c \\ k_q \dfrac{q_\alpha q_\beta}{r} & r \geq r_c \end{cases} \quad (3)$$

where $U_{\alpha\beta}^{\mathrm{vdW}}(r)$ is the van der Waals interaction between sites α and β separated by a distance r, q_α is the charge on site α, $k_q = 1/4\pi\epsilon_0$ where ϵ_0 is the permittivity of vacuum, and the cutoff $r_c = 12$ Å. The charges on each atom are defined such that each Si atom has a partial charge of $0.3e$ times the number of O atoms directly bonded to it and each O atom has a partial charge of $-0.3e$ times the number of Si atoms directly bonded to it, where e is the proton charge. Since the CH_3 groups have zero partial charge, this yields a molecule with no net charge. For van der Waals interactions between Si or O atoms, the 9−6 potential is used

$$U_{\alpha\beta}^{\mathrm{vdW}}(r) = \epsilon_{\alpha\beta}\left[2\left(\frac{\sigma_{\alpha\beta}}{r}\right)^9 - 3\left(\frac{\sigma_{\alpha\beta}}{r}\right)^6\right], \quad \alpha \text{ and } \beta = \{\mathrm{Si, O}\} \quad (4)$$

where the parameters for $\epsilon_{\alpha\beta}$ and $\sigma_{\alpha\beta}$ are given in Table 1. For interactions involving CH_3 groups, a 12−6 potential is used

$$U_{\alpha\beta}^{\mathrm{vdW}}(r) = 4\epsilon_{\alpha\beta}\left[\left(\frac{\sigma_{\alpha\beta}}{r}\right)^{12} - \left(\frac{\sigma_{\alpha\beta}}{r}\right)^6\right], \quad \alpha \text{ or } \beta = \mathrm{CH_3} \quad (5)$$

Covalent bond stretching and bending potentials are modeled using harmonic potentials

$$U_{\mathrm{bond}}(r) = \frac{1}{2}k_{\mathrm{bond}}(r - r_0)^2 \quad (6)$$

with spring constant k_{bond} and equilibrium bond distance r_0 and

$$U_{\mathrm{bend}}(\theta) = \frac{1}{2}k_{\mathrm{bend}}(\theta - \theta_0)^2 \quad (7)$$

Table 1. Potential Parameters for the Hybrid/UA Model of PDMS[32]

van der Waals	$\epsilon_{\alpha\beta}$ [kcal/mol]	$\sigma_{\alpha\beta}$ [Å]
Si−Si	0.1310	4.29
Si−O	0.0772	3.94
Si−CH_3	0.1596	3.83
O−O	0.0800	3.30
O−CH_3	0.1247	3.38
CH_3−CH_3	0.1944	3.73
bonds	k_{bond} [kcal/(mol Å^2)]	r_0 [Å]
Si−O	350.12	1.64
Si−C H_3	189.65	1.90
angles	k_{bend} [kcal/(mol rad^2)]	θ_0 [deg]
Si−O−Si	14.14	146.46
O−Si−O	94.5	107.82
C H_3−Si−C H_3	49.97	109.24
O−Si−C H_3	49.97	110.69
dihedrals	k_{tors} [kcal/mol]	n
Si−O−Si−O	0.225	1
Si−CH_3−Si−CH_3	0.01	3

with equilibrium bend angle θ_0. The torsional potentials are of the form

$$U_{tors}(\phi) = k_{tors}[1 + \cos(n\phi)] \tag{8}$$

where $\phi = \pi$ corresponds to the trans state. The parameters for these potentials are summarized in Table 1.

Molecular dynamics simulations were performed on OH-terminated PDMS melts containing 1000 chains of PDMS with $N = 40$ monomers per chain with 400, 500, or 600 cross-linkers and 2000 chains of $N = 20$ PDMS with 1000 cross-linker molecules, giving two systems with a stoichiometric amount of cross-linkers and one system with either an excess of cross-linker molecules or an excess of chains. All simulations were performed at a temperature $T = 400$ K. Each system was initially formed by randomly attaching a specified number of cross-linkers to PDMS chain ends and inserting the PDMS chains, each with up to two cross-linkers attached, into a cubic box with random orientations. The dimensions of the simulation cells were $L = 186$ Å for the $N = 20$ system and approximately $L = 182$ Å for the three $N = 40$ systems, giving a fixed density of 0.86 g/cm^3 for each system. We used a multiple time step second-order symplectic integrator (RESPA)[33] to solve the equations of motion. The long-range Coulomb interactions were calculated using a particle−particle/particle−mesh Ewald (PPPM) algorithm.[34] The temperature was kept constant by using a Langevin thermostat with a damping constant of 0.01 fs^{-1}.[35] The simulations were run with a 2 fs time step for the bond length fluctuations, 4 fs time step for the angle, torsion, and improper forces, and an 8 fs time step for the van der Waals forces. For the system with 1000 chains of length $N = 40$ with 500 cross-linkers, simulating 1 ns using the LAMMPS code[36] took approximately 30 h on 48 processors of Sandia's CPlant DEC alpha cluster or 15 h on 36 processors of an Intel Xeon cluster.

Since the chains initially overlapped, we applied the bonded potentials along with a soft nonbonded potential defined as

$$U_{soft}(r) = \begin{cases} A(1 + \cos(\pi r/r_c)) & r \le r_c \\ 0 & r > r_c \end{cases} \tag{9}$$

with $r_c = 2^{1/6}\sigma_{\alpha\beta}$ defined separately for each $\alpha\beta$ pair. The amplitude A increased linearly from 1.0 to 500.0 kcal/mol over the course of 10 ps. This allowed all of the overlapping chains to be pushed apart quickly but smoothly. At this point, the full nonbonded potential was applied, and each system was equilibrated for 2.0 ns at a density of 0.86 g/cm^3.

3. Network Formation

The cross-linking reaction is performed by forming a bond between one of the remaining terminal SiH united atoms on the cross-linker and the nearest terminal OH united atom on the PDMS chain. The bond forms with unit probability when the SiH and OH united atoms come within a reaction radius r_x of each other. Since the atomic diameters of SiH and OH are 4.29 and 3.30 Å, respectively, the nonbonded SiH and OH united atoms can never approach their equilibrium bond distance of 1.64 Å due to the strong repulsion of the 9−6 and 12−6 potentials for $r < \sigma_{\alpha\beta}$. Therefore, we define a reaction to occur when the two united atoms are separated by $r_x = 6.5$ Å and define a new bond potential specifically for the formation of cross-links. This new bond potential is necessary since the harmonic bond potential, eq 6, is quite large for this large bond separation and would lead to instabilities. The new cross-link bond potential, shown in eq 10, is harmonic at bond distances below r_{cut} and linear at large distances.

$$U_{bond}^{xlink}(r) = \begin{cases} \frac{1}{2}k_{bond}(r - r_0)^2 & r \le r_{cut} \\ \frac{1}{2}k_{bond}(r_{cut} - r_0)^2 + \frac{1}{2}k'_{bond}(r - r_{cut}) & r > r_{cut} \end{cases} \tag{10}$$

In eq 10, k'_{bond} is set to 35.01 kcal/mol and $r_{cut} = 1.71$ Å. This allows the Si and O atoms to be pulled together with a constant force of 17.5 kcal/(mol Å) until the bond energy is below 1 k_BT. When a bond forms, the van der Waals interaction between united atoms separated by less than four bonds is turned off, and the new angular potentials are added to the newly cross-linked molecule without modifying the harmonic angle bending potential.

The time required to form the network from the melt is strongly dependent on the chain length and cross-linker stoichiometry. Achieving 85% conversion takes from 6 to 15 ns for the systems studied here. As the network formation nears complete conversion, the rate of bond formation decreases to the point where it is no longer practical to simulate. Once the rate of network formation slows to where tens of thousands of steps are required to form a single additional bond, the simulation is stopped. To form a more complete network in a short amount of time, the reaction radius for bond formation is extended to $r_x = 10$ Å. In addition, the temperature is ramped up to 1000 K over a period of 10 ps and back down to 400 K over 10 ps using the Langevin thermostat while maintaining zero pressure. Once returned to $T = 400$ K, the simulation is run for an additional 10 ps to allow the volume to reequilibrate. The density of each system after network formation is listed in Table 2. Although this procedure does not provide kinetic information, it allows nearby sites to form bonds that would likely have formed if the simulations were run longer. This results in an additional 35−51 bonds formed for

Table 2. Network Formation Characteristics of Each System[a]

N_x	N_c	N	N_{tot}	ρ [g/cm^3]	p
400	1000	40	167 800	0.9175	90.9
500	1000	40	169 500	0.9061	86.4
600	1000	40	171 200	0.9564	91.6
1000	2000	20	179 000	0.9671	94.0

[a] N_x is the number of cross-linkers in the system, N_c the number of chains, N the number of monomers per chain, and N_{tot} the total number of sites in the system. The density is ρ, and p is the percent conversion of free chain ends to bonds.

the $N = 40$ systems and 207 new bonds formed for the $N = 20$ system. The final percent conversion for these simulations ranges from 86% to 94%, comparable to experimental networks.

3.1. Formation Kinetics. The kinetics of network formation can be loosely characterized as a reaction where two free species A and B combine to form a third inert species. In this case, the kinetics depend on whether a stoichiometric amount of species A and B is present. For the stoichiometric case, the concentration of reactants decays as $1/t$, while for the nonstoichiometric case, it decays exponentially.[25] Kang and Redner[37] found that for dimensionalities $d < d_c = 4$ concentration fluctuations determine the kinetics when such a reaction is diffusion limited. Concentration fluctuations lead to domains with excess amounts of one species such that after times proportional to l^2, where l is the linear dimension of the domain size, only the excess species remains. They find that this leads to an overall decay rate of $t^{-d/4}$ when equal amounts of species A and B are present initially.

For network formation, the rate constant of diffusion-controlled processes is time dependent since the chain motion is diffusive only after a time $\tau_R \sim N^2$ where τ_R is the Rouse time and N is the chain length. The rate constant scales as $t^{-3/8}$ for $t < \tau_R$ and as $t^{-1/4}$ for $t > \tau_R$.[38] For chains longer than the entanglement length ($N_e \approx 160$ for PDMS at 300 K[39]), the rate constant would be independent of time when t is larger than the reptation time.[40] Since the motion at early times is Rouse-like, the number of free ends should decay as[25,26]

$$N_f(t) \sim t^{-d/8}, \quad d \le d_c = 8 \tag{11}$$

The nonstoichiometric case is more complicated as one species is consumed more rapidly than the other resulting in nonsymmetric concentration fluctuations.

Table 2 presents the network characteristics after completion of the network formation and volume equilibration. The simulated network formation kinetics are shown in Figure 2. Here, the number of unreacted cross-linking sites divided by the total number of cross-linking sites is plotted as a function of time. For the case where excess cross-linking sites are present, the excess is subtracted from both numbers. Each system shows a power law decay at long times with exponents of 0.29 $\pm$ 0.02 and 0.33 $\pm$ 0.02 for the $N = 20$ and $N = 40$ stoichiometric cases, respectively, slightly below the value predicted by eq 11. Since the PDMS chains studied here are too short to be Gaussian, the slow reaction rate may be due to the inability of the dangling ends to diffuse close enough to each other to form a bond. The results are, however, in better agreement with eq 11 than earlier simulations[13,26] forming networks of bead−spring chains. In these earlier simulations, the power law exponent was found to be ~0.5 for the stoichiometric case. For the nonstoichiometric cases, the decay rates are faster than the stoichiometric cases due to the excess amount of cross-linkers or chains present.

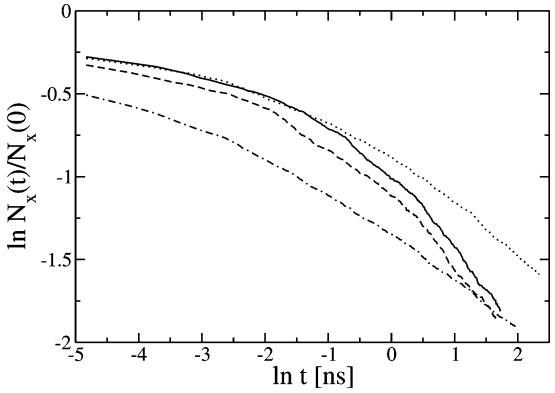

Figure 2. Number of free cross-linking sites remaining divided by the initial number of free cross-linking sites for the PDMS networks as defined in Table 2 for $N_x = 400$ (solid line), 500 (dotted), 600 (dashed), and 1000 (dot−dashed).

The chain dimensions before and after cross-linking are shown in Table 3. Here, $\langle R^2 \rangle$ is the mean-squared end-to-end distance, and $\langle R_g^2 \rangle$ is the mean-squared radius of gyration of the chains in the melt or the strands in the network. The cross-linkers are not included in the calculation of these values. The subscripts m and n correspond to the melt and the fully formed network, respectively. Upon forming the network, the end-to-end distance of the chains decreases by an average of 16% and the radius of gyration decreases by an average of 8%. This contrasts with earlier simulations using bead−spring models[13,14] as well as small-angle neutron scattering (SANS) experiments[41] on longer hydride-terminated PDMS chains ranging from $N = 86$ to $N = 337$ that saw almost no change in the chain dimensions after networking. However, the ratio $\langle R^2 \rangle / \langle R_g^2 \rangle$ is significantly larger than the value of 6 expected for random walk statistics for melts. Even though the chains in the melt have equilibrated, they are non-Gaussian because of their intrinsic structure whereas the chains in the bead−spring model studied previously and the SANS experiments were Gaussian. The decrease in chain dimensions may be due to the fact that, once a bond forms, the united atom pairs between the two chains that are now separated by less than four bonds interact with bond and angle potentials instead of van der Waals potentials. In united atom models, this brings the atoms closer together whereas in bead−spring models, sites usually do not overlap even when bonded to each other. Also, the effect on the end-to-end distance and radius of gyration diminishes as the chain length increases, making it difficult to detect for chains long enough to exhibit Gaussian behavior. The change in chain dimensions and non-Gaussian behavior seen in these more realistic models are features that are not included in network theories that assume Gaussian statistics apply, including the affine and phantom models.

4. Uniaxial Elongation

The elastic modulus of polymer networks is easily measured from dynamic mechanical experiments. For simulations, the modulus can be obtained in a similar manner from uniaxial elongation of the network. After the chains are cross-linked and the density equilibrates

Table 3. Chain Dimensions of the Melt (*m*) and Network (*n*) for Each System As Defined in Table 2[a]

N_x	N	$\langle R^2\rangle_m$	$\langle R^2\rangle_n$	$\langle R_g^2\rangle_m$	$\langle R_g^2\rangle_n$	$\langle R^2\rangle_m/\langle R_g^2\rangle_m$	$\langle R^2\rangle_n/\langle R_g^2\rangle_n$
400	40	3214(31)	2728(35)	362(3)	332(3)	8.9(1)	8.2(1)
500	40	3334(33)	2844(37)	366(3)	347(3)	9.1(1)	8.2(1)
600	40	3250(29)	2759(35)	364(3)	339(3)	8.9(1)	8.1(1)
1000	20	1028(9)	847(9)	140(1)	124(1)	7.3(1)	6.8(1)

[a] $\langle R^2\rangle$ is the mean-squared end-to-end distance, and $\langle R_g^2\rangle$ is the mean-squared radius of gyration of the chains in the melt or the strands in the network. The subscripts *m* and *n* correspond to the melt and the fully formed network, respectively.

to the values listed in Table 2, the bond formation mechanism is turned off, and the bond formation potential, $U_{\text{bond}}^{\text{xlink}}(r)$, is replaced with the harmonic potential, $U_{\text{bond}}(r)$. At this point, the dihedral interactions due to the newly formed bonds are manually added to the simulations. Each simulation is then equilibrated at fixed volume for 1 ns before applying a strain.[42]

The simulation cell starts as a cube of dimension L. At $t = 0$, the cell undergoes a constant volume extension in the z direction at a constant rate $\dot{\epsilon}_0$ according to

$$L_\alpha(t) = \lambda_\alpha(t)L \tag{12}$$

where

$$\lambda_z(t) = \lambda(t) = (1 + \dot{\epsilon}_0 t)$$

$$\lambda_x(t) = \lambda_y(t) = \lambda(t)^{-1/2} \tag{13}$$

Each system is strained for 0.5 ns at a time step of 5 fs at four different strain rates, $\dot{\epsilon}_0 = 0.4$, 0.6, 1.0, and 2.0 ns^{-1}, resulting in final extensions of $\lambda = 1.2$, 1.3, 1.5, and 2.0.

4.1. Stress/Strain Behavior. The components of the stress tensor are defined as

$$V\sigma_{\alpha\beta} = -\sum_i m_i v_{i,\alpha} v_{i,\beta} + \frac{1}{3N}\sum_{i\neq j} F_{ij,\alpha} \cdot r_{ij,\beta} \tag{14}$$

where V is the volume, m_i is the mass and $v_{i,\alpha}$ is the α component of the velocity of atom i, $F_{ij,\alpha}$ is the α component of the force between atoms i and j, and $r_{ij,\beta}$ is the β component of vector $\mathbf{r}_i - \mathbf{r}_j$ between atoms i and j. For uniaxial tension in the z direction, the tensile stress is defined as

$$\sigma_T = \sigma_{zz} - \frac{\sigma_{xx} + \sigma_{yy}}{2} \tag{15}$$

From classical viscoelasticity theory, this is related to the strain according to

$$\sigma_T = G_e\left(\lambda^2 - \frac{1}{\lambda}\right) \tag{16}$$

Other models, such as the tube model of Heinrich and Straube,[43] a variant of this by Rubinstein and Panyukov,[44] or the double-tube model of Mergell and Everaers,[20] have been shown to be more accurate.

The tensile stress for the $N = 20$ system at four different strain rates is shown in Figure 3. The strain is increased linearly for the first 0.5 ns and then maintained at a fixed value for the remainder of each simulation. The standard deviation in the tensile stress data is roughly 100 atm for each data set. Note that the data show a nonlinear regime during the latter part of the straining period at high strain rates, indicative of the connectivity of the network.

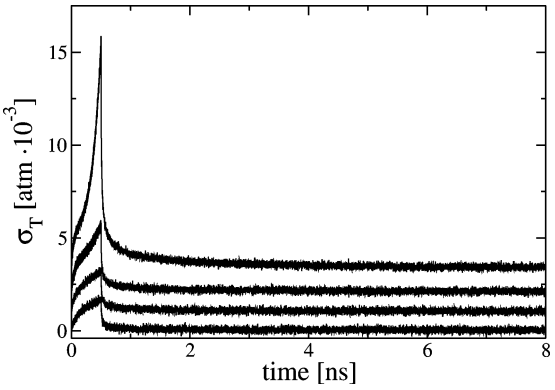

Figure 3. Tensile stress for the 1000 cross-linker system at four different strain rates, $\dot{\epsilon} = 2.0$, 1.0, 0.6, and 0.4 ns^{-1} from top to bottom. For each simulation, the strain is applied for a duration of 0.5 ns followed by relaxation at fixed strain. The relaxation data is recorded for up to 20 ns to ensure that an accurate plateau value is obtained. The data sets are shifted vertically for clarity.

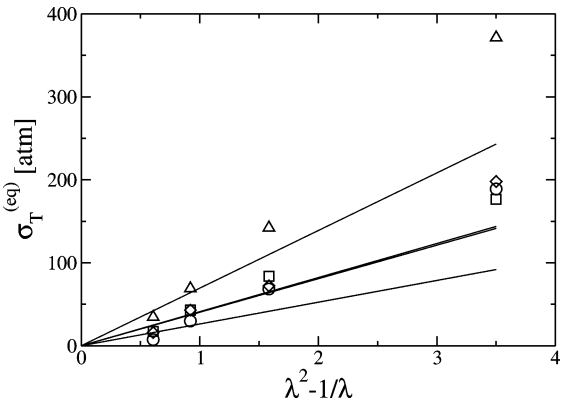

Figure 4. Equilibrium tensile stress for end-cross-linked networks. The symbols correspond to the systems with 400 (circles), 500 (squares), 600 (diamonds), and 1000 cross-linkers (triangles), as defined in Table 2. The lines are linear fits to the lowest two data points constrained to pass through the origin.

4.2. Elastic Modulus. As seen in Figure 3, the tensile stress decays to a plateau after several nanoseconds. The plateau value of the stress is obtained by fitting the Prony series

$$\sigma_T(t) = G_0(1 - \sum_{i=1}^{N_i} p_i(1 - \mathrm{e}^{-t/\tau_i})) \tag{17}$$

to the tensile stress data for the relaxation period and extracting the quantity $G_0(1 - \sum_{i=1}^{N_i} p_i)$. The fits are performed using a nonlinear least-squares fitting procedure with $N_i = 2$ terms in the series. The plateau value of the tensile stress for each system, $\sigma_T^{(\text{eq})}$, is plotted as a function of the normalized strain in Figure 4. From eq 16, the slope of this curve in the small strain region gives the plateau modulus for the network. The

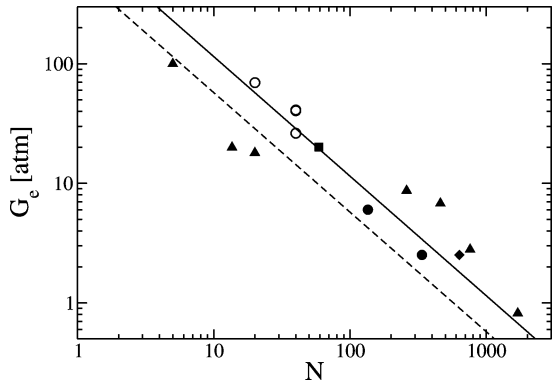

Figure 5. Elastic modulus for end-cross-linked PDMS obtained from simulation (open symbols) and experiment (closed circles,[45] squares,[47] diamonds,[46] and triangles[48]). The solid line represents the affine model, and the dashed line represents the phantom model with a stoichiometric amount of cross-linkers.

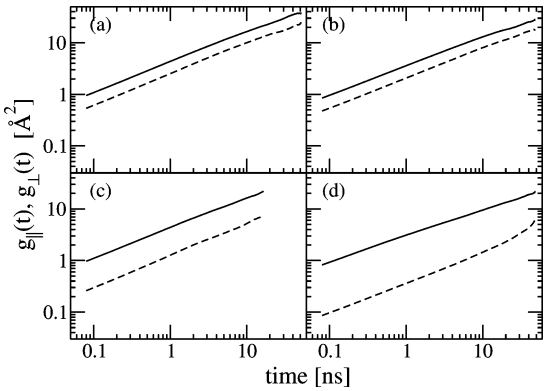

Figure 6. Components of the mean-square displacement of saturated cross-linker molecules in the direction parallel (dashed line) and perpendicular (solid line) directions. The curves are for the stoichiometric systems with (a) $N = 40$, $\lambda = 1.2$; (b) $N = 20$, $\lambda = 1.2$; (c) $N = 40$, $\lambda = 2.0$; and (d) $N = 20$, $\lambda = 2.0$. Time zero corresponds to 2.5 ns after the strain is applied.

nonlinear behavior at the two highest strain rates prevents us from including these data points in the fit for the plateau modulus. Combined with the uncertainty in the remaining data points, roughly equal to the symbol size, deviations from classical viscoelasticity theory, such as in a Mooney−Rivlin plot or a fit to tube models,[20,43,44] are difficult to access. Comparing the two symmetric systems, we find that the large strand length dependence of the tensile stress exceeds the $1/N_s$ behavior predicted by the models. The tensile stress of the $N = 20$ system is 6−8 times greater than the $N = 40$ system at the same strain rate.

Figure 5 compares these values to experimental results[45−48] at room temperature for vinyl-terminated PDMS networks end cross-linked with tetrakis(dimethylsiloxy)silane. The experimental data are limited to networks prepared in the bulk to avoid swelling effects, which tend to decrease the number of trapped entanglements.[49] The solid and dashed lines correspond to the predictions of the affine model (eq 1) and the phantom model (eq 2), respectively. For these two models, we use the fact that the tensile modulus is 3 times the shear modulus in the limit of small strain for isotropic materials. Here, the phantom model assumes a stoichiometric amount of cross-linker such that $\mu = \nu/2$. The simulation results are in qualitative agreement with the experimental data and within the same range of the classical models, although both the simulation and experimental data demonstrate the difficulty of obtaining consistent results as well as the sensitivity to variables other than the strand length and number of cross-linkers.

Besides bulk behavior, the simulations also allow the local structure and dynamics of the network to be characterized. Figure 6 presents the components of the mean-square displacement, $g_\alpha(t) = \langle (R_\alpha(t) - R_\alpha(0))^2 \rangle$, of the center silicon atom of each cross-linker molecule that is bonded to four network strands in the direction parallel and perpendicular to the strain. Here, $g_\perp(t) = (g_x(t) + g_y(t))/2$. The data are collected after each system is strained and allowed to relax for 2.5 ns. The curves follow a $t^{1/2}$ power law, which is the expected Rouse-like behavior at short times. These curves are expected to reach a plateau value at late times due to the constrained motion of the cross-linker molecules in the network, but that is not seen for the duration of these simulations. The cross-linker mobility is larger in the direction perpendicular to the strain, which is opposite to the standard results[13,24,26,50] for Gaussian strands. When a strain is applied to tube models, the tube dimensions increase in the direction parallel to the strain and decrease in the perpendicular direction. Thus, the cross-linkers have greater mobility in the parallel direction. However, for the networks studied here, the short strand length causes the strands to be stretched to the point where bonding constraints hinder the cross-linker mobility in the parallel direction. This effect is enhanced going from the $N = 40$ strand length (Figure 6c) to the $N = 20$ strand length (Figure 6d).

4.3. Chain Dimensions in Deformed Networks. Chain conformations in uniaxially stretched networks have been studied using SANS by taking advantage of the dependence of the scattering form factor on the mean-square radius of gyration. The components of the radius of gyration parallel and perpendicular to the strain direction can be obtained from the scattering intensities in these directions. Scattering laws have been derived from polymer network models,[51−53] allowing a direct comparison between experiment and theory for the chain conformations in deformed networks.

The chain deformation in the affine model is given by[51]

$$R_{g,\parallel}/R_{g,i} = \lambda \tag{18}$$

$$R_{g,\perp}/R_{g,i} = \lambda^{-1/2} \tag{19}$$

where $R_{g,\parallel}$ and $R_{g,\perp}$ are the components of the radius of gyration parallel and perpendicular to the stretching direction, respectively, and $R_{g,i}$ is the same component for the unstretched network. For the phantom model, the chain deformation is given by[52]

$$R_{g,\parallel}/R_{g,i} = \left(\frac{f + 2 + (f-2)\lambda^2}{2f}\right)^{1/2} \tag{20}$$

$$R_{g,\perp}/R_{g,i} = \left(\frac{f + 2 + (f-2)\lambda^{-1}}{2f}\right)^{1/2} \tag{21}$$

where f is the functionality of the cross-linker molecules.

The components of the radius of gyration are obtained from the simulations by directly measuring the atomic coordinates for each chain that has reacted with two cross-linkers. In other words, no dangling ends are

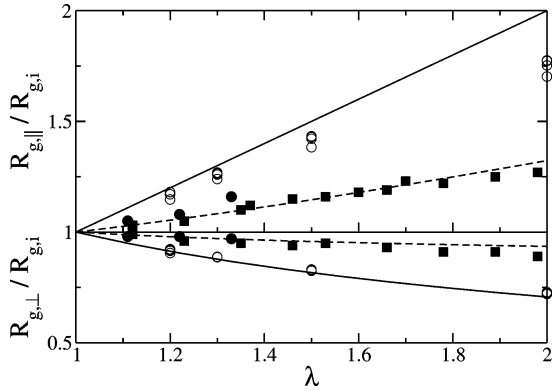

Figure 7. Variation of components of the radius of gyration parallel and perpendicular to the strain direction. Open symbols are simulation data. Closed symbols are data from SANS experiments[45] for $N = 80$ (circles) and $N = 135$ (squares). The solid and dashed lines are the affine and phantom models, respectively.

included in the calculation. The results are compared to the affine and phantom models in Figure 7, along with SANS data[45] for end-linked hydride-terminated PDMS networks prepared in the bulk. The figure clearly demonstrates that our short chains follow the affine model whereas the experimental data are much closer to the phantom model. This is most likely a consequence of the strand length where the shorter strands require the cross-links to follow the bulk deformation, in agreement with the affine model. Longer strands offer more cross-linker mobility, which allows them to move more independently of the bulk deformation, as in the phantom model.

5. Conclusions

This paper presents the first united atom model simulation of the network formation and elongation of model PDMS networks formed with tetrafunctional cross-linkers. Compared to earlier simulations using bead−spring models, several differences are observed. Here, the formation kinetics for stoichiometric systems exhibit a $t^{-0.3}$ scaling, in closer agreement to the predicted $t^{-0.375}$ rate for Rouse-like chain motion. Whereas earlier simulations found almost no change in the chain dimensions after networking, we find that for the relatively short PDMS chains studied here the end-to-end distance decreases by an average of 16% and the radius of gyration decreases by an average of 8%. We attribute at least part of this decrease in chain length to the fact that the chains studied here are non-Gaussian.

Each networked system is uniaxially strained at four different strain rates. After the network is strained, the tensile stress is allowed to relax to a plateau value over tens of nanoseconds. From the stress−strain cure, we extract the elastic modulus. The results are in qualitative agreement with experimental measurements of model end-linked PDMS networks. The change in chain dimensions after straining are in accordance with the affine model predictions whereas experimental results follow the phantom model predictions. This may be partially due to the smaller chain length in the simulation.

This paper demonstrates the feasibility of applying massively parallel molecular dynamics simulation to the study of polymer network formation and stress relaxation at the united atom level. Current computational abilities are sufficient to capture the classical viscoelastic behavior of polymer networks. An additional order of magnitude increase in computational power will make accessible chain lengths on the order of the entanglement length, making direct comparison with several experimental studies including SANS and dynamic mechanical experiments. Future work will also include studying the effects of cross-linking near surfaces and extending the model to include vinyl-terminated PDMS.

Acknowledgment. Sandia is a multiprogram laboratory operated by Sandia Corporation, a Lockheed Martin Company, for the United States Department of Energy's National Nuclear Security Administration under Contract DE-AC04-94AL85000.

References and Notes

(1) Wall, F. T. *J. Chem. Phys.* **1943**, *11*, 527.
(2) Flory, P. J. *Principles of Polymer Chemistry;* Cornell University Press: Ithaca, NY, 1953.
(3) James, H. M.; Guth, E. *J. Chem. Phys.* **1947**, *15*, 669.
(4) Gottlieb, M.; Gaylord, R. J. *Polymer* **1983**, *24*, 1644.
(5) Gottlieb, M.; Gaylord, R. J. *Macromolecules* **1984**, *17*, 2024.
(6) Mark, J. E.; Erman, B. *Rubberlike Elasticity: A Molecular Primer;* Wiley-Interscience: New York, 1988.
(7) Ronca, G.; Allegra, G. *J. Chem. Phys.* **1975**, *63*, 4990.
(8) Flory, P. J. *J. Chem. Phys.* **1977**, *66*, 5720.
(9) Flory, P. J.; Erman, B. *Macromolecules* **1982**, *15*, 800.
(10) Mark, J. E. *Adv. Polym. Sci.* **1982**, *44*, 1.
(11) Pearson, D. S.; Graessley, W. W. *Macromolecules* **1980**, *13*, 1001.
(12) Gottlieb, M.; Macosko, C. W.; Benjamin, G. S.; Meyers, K. O.; Merrill, E. W. *Macromolecules* **1981**, *14*, 1039.
(13) Duering, E. R.; Kremer, K.; Grest, G. S. *J. Chem. Phys.* **1994**, *101*, 8169.
(14) Kenkare, N. R.; Smith, S. W.; Hall, C. K.; Khan, S. A. *Macromolecules* **1998**, *31*, 5861.
(15) Grest, G. S.; Pütz, M.; Everaers, R.; Kremer, K. *J. Non-Cryst. Solids* **2000**, *274*, 139.
(16) Chen, Z.; Escobedo, F. A.; Cohen, C. *Macromolecules* **2002**, *35*, 3296.
(17) Svaneborg, C.; Grest, G. S.; Everaers, R., to be published.
(18) Edwards, S. F. *Proc. Phys. Soc.* **1967**, *92*, 9.
(19) Edwards, S. F. *Polymer* **1977**, *9*, 140.
(20) Mergell, B.; Everaers, R. *Macromolecules* **2001**, *34*, 5675.
(21) Everaers, R.; Kremer, K. *Macromolecules* **1995**, *28*, 7291.
(22) Sivasailam, K.; Cohen, C. *J. Rheol.* **2000**, *44*, 897.
(23) Roth, L. E.; Vallés, E. M.; Villar, M. A. *J. Polym. Sci., Part A* **2003**, *41*, 1099.
(24) Duering, E. R.; Kremer, K.; Grest, G. S. *Phys. Rev. Lett.* **1991**, *67*, 3531.
(25) Grest, G. S.; Kremer, K.; Duering, E. R. *Europhys. Lett.* **1992**, *19*, 195.
(26) Grest, G. S.; Kremer, K.; Duering, E. R. *Physica A* **1993**, *194*, 330.
(27) Gao, J.; Weiner, J. H. *J. Chem. Phys.* **1995**, *103*, 1614.
(28) Trautenberg, H.; Sommer, J.-U.; Göritz, D. *J. Chem. Soc., Faraday Trans.* **1995**, *91*, 2649.
(29) Escobedo, F. A.; de Pablo, J. J. *J. Chem. Phys.* **1996**, *104*, 4788.
(30) Escobedo, F. A.; de Pablo, J. J. *J. Chem. Phys.* **1997**, *106*, 793.
(31) Hölzl, T.; Trautenberg, H. L.; Göritz, D. *Phys. Rev. Lett.* **1997**, *79*, 2293.
(32) Frischknecht, A. L.; Curro, J. G. *Macromolecules* **2003**, *36*, 2122 In Table 1 of this paper, the angle energy parameters k_θ should have units of kcal/mol/rad^2, not kcal/mol/deg^2 as written (Frischknecht, private communication).
(33) Tuckerman, M.; Berne, B. J.; Martyna, G. J. *J. Chem. Phys.* **1990**, *92*, 5057.
(34) Hockney, R.; Eastwood, J. *Computer Simulation using Particles;* Adam Hilger: New York, 1988.
(35) Grest, G. S.; Kremer, K. *Phys. Rev. A* **1986**, *33*, 3628.
(36) Plimpton, S. *J. Comput. Phys.* **1995**, *117*, 1.
(37) Kang, K.; Redner, S. *Phys. Rev. A* **1985**, *32*, 435.
(38) de Gennes, P. G. *J. Chem. Phys.* **1982**, *76*, 3316.
(39) Fetters, L. J.; Lohse, D. J.; Milner, S. T.; Graessley, W. W. *Macromolecules* **1999**, *32*, 6847.
(40) de Gennes, P. G. *J. Chem. Phys.* **1982**, *76*, 3322.

(41) Beltzung, M.; Picot, C.; Rempp, P.; Herz, J. *Macromolecules* **1982**, *15*, 1594.
(42) The chain dimensions for the networks listed in Table 3 are obtained after the dihedral interactions are added and the systems are equilibrated. If the dihedral interactions are left out, the chain dimensions are the same within the uncertainty of the measurement.
(43) Heinrich, G.; Straube, E.; Helmis, G. *Adv. Polym. Sci.* **1988**, *85*, 34.
(44) Rubinstein, M.; Panyukov, S. *Macromolecules* **1997**, *30*, 8036.
(45) Beltzung, M.; Picot, C.; Herz, J. *Macromolecules* **1984**, *17*, 663.
(46) Urayama, K.; Kohjiya, S. *J. Chem. Phys.* **1996**, *104*, 3352.
(47) Urayama, K.; Kawamura, T.; Kohjiya, S. *J. Chem. Phys.* **1996**, *105*, 4833.
(48) Schroeder, M. J.; Roland, C. M. *Macromolecules* **2002**, *35*, 2676.
(49) Candau, S.; Peters, A.; Herz, J. *Polymer* **1981**, *22*, 1504.
(50) Duering, E. R.; Kremer, K.; Grest, G. S. *Macromolecules* **1993**, *26*, 3241.
(51) Benoit, H.; Duplessix, R.; Ober, R.; Daoud, M.; Cotton, J. P.; Farnoux, B.; Jannink, G. *Macromolecules* **1975**, *8*, 451.
(52) Pearson, D. *Macromolecules* **1977**, *10*, 696.
(53) Erman, B. *Macromolecules* **1987**, *20*, 1917.

MA035760J